doi:10.1093/brain/awq144 Brain 2010: 133; 2007–2021 | 2007

BRAIN
A JOURNAL OF NEUROLOGY

Subthalamic span of β oscillations predicts deep brain stimulation efficacy for patients with Parkinson's disease

Adam Zaidel,[1,2] Alexander Spivak,[3] Benjamin Grieb,[4] Hagai Bergman[1,2] and Zvi Israel[3]

1 The Interdisciplinary Centre for Neural Computation, The Hebrew University of Jerusalem, Jerusalem 91904, Israel
2 Department of Medical Neurobiology (Physiology), Canada-Israel Institute for Medical Research, The Hebrew University Hadassah Medical School, Jerusalem 91120, Israel
3 Centre for Functional & Restorative Neurosurgery, Department of Neurosurgery, Hadassah University Hospital, Jerusalem 91120, Israel
4 Department of Neurophysiology and Pathophysiology, University Medical Centre Hamburg-Eppendorf, Hamburg 20246, Germany

Correspondence to: Adam Zaidel,
Department of Medical Neurobiology (Physiology),
Canada-Israel Institute for Medical Research,
The Hebrew University Hadassah Medical School,
P.O. Box 12272, Jerusalem 91120, Israel
E-mail: adam@alice.nc.huji.ac.il

The significance of oscillations that characterize the subthalamic nucleus in Parkinson's disease is still under debate. Here, we analysed the spectral and spatial characteristics of 314 microelectrode trajectories from 128 patients undergoing subthalamic nucleus deep brain stimulation surgery for Parkinson's disease. We correlated the subthalamic nucleus pathophysiology with the outcome of surgery, as evaluated by the third section of the Unified Parkinson's Disease Rating Scale (motor score), which was subdivided into tremor, rigidity, limb-bradykinesia and axial-bradykinesia subscores. β-oscillatory activity (13–30 Hz) comprised a continuous stretch within the subthalamic nucleus, and was limited to a distinctly-bounded dorsolateral oscillatory region. Although less consistent and more sporadic, low-frequency (3–7 Hz) power was also increased in the dorsolateral oscillatory region. In contrast, the more ventral subthalamic nucleus was characterized by consistently reduced β and increased gamma (30–100 Hz) activity. Neuronal responses to passive arm movement (analysed by their alignment to goniometer tracing of the joints' angular displacement) were significantly more common in the dorsolateral oscillatory region than the ventral subthalamic nucleus region (62 versus 25% of sites tested respectively, $P<0.01$). The length of the dorsolateral oscillatory region recorded in the macroelectrode-implanted trajectory predicted a favourable response to subthalamic nucleus deep brain stimulation ($R=0.67$, $P<0.0001$). This correlation was also evident for improvement in the specific symptom subscores of rigidity, limb-bradykinesia and axial-bradykinesia ($P<0.05$). Similarly, increased subthalamic nucleus β power was associated with postoperative improvement. In contrast, the preoperative response to levodopa did not correlate with dorsolateral oscillatory region length ($P=0.33$), however, it did tend to be associated with increased β (and decreased low frequency) subthalamic nucleus power. Finally, the active macroelectrode contact, independently selected by optimal clinical outcome, coincided with the dorsolateral oscillatory region centre. On average, the location of the active contact was not significantly different from the dorsolateral oscillatory region centre ($P=0.10$), but was significantly different from the subthalamic nucleus centre ($P<0.0001$). We conclude that the spatial extent of the dorsolateral oscillatory region, which overlaps the motor territories of the subthalamic nucleus, predicts the outcome of subthalamic nucleus deep brain stimulation. Thus the frequency and spatial characteristics of the subthalamic nucleus trajectory may be used for deep brain stimulation outcome optimization.

Received March 8, 2010. Revised April 19, 2010. Accepted May 3, 2010. Advance Access publication June 9, 2010

Keywords: basal ganglia; subthalamic nucleus; Parkinson's disease; beta oscillations; power spectral density

Abbreviations: DBS = deep brain stimulation; NRMS = normalized root mean square; RMS = root mean square; STN = subthalamic nucleus; UPDRS = Unified Parkinson's Disease Rating Scale

Introduction

Midbrain dopaminergic neurons and their projections to the basal ganglia degenerate in Parkinson's disease (Bernheimer *et al*., 1973), leading to a cascade of physiological abnormalities in the basal ganglia. Primary studies on the primate (Miller and DeLong, 1987; Filion and Tremblay, 1991; Bergman *et al*., 1994; Nini *et al*., 1995) and rodent (Magill *et al*., 2001; Costa *et al*., 2006) models of Parkinson's disease have demonstrated changes in firing rates, increased synchrony and exaggerated oscillations in the parkinsonian basal ganglia—particularly in the subthalamic nucleus (STN) and the internal segment of the globus pallidus.

Neuronal recording from the human basal ganglia has become possible due to surgical treatment for advanced Parkinson's disease, such as deep brain stimulation (DBS) of the STN (Limousin *et al*., 1995; Krack *et al*., 2003; Machado *et al*., 2006). During surgery for implanting an STN DBS macroelectrode, microelectrode recording is often utilized to verify localization of the STN physiologically (Sterio *et al*., 2002; Israel and Burchiel, 2004; Gross *et al*., 2006). In addition, during or shortly after surgery, local field potentials can be recorded from the implanted macroelectrodes before their connector is internalized and connected to a pulse generator (Kuhn *et al*., 2005; Chen *et al*., 2006). These physiological studies have focused attention toward pathological β (13–30 Hz) oscillatory activity in the STN of patients with Parkinson's disease (Levy *et al*., 2000; Brown *et al*., 2001; Marceglia *et al*., 2006*a*).

Although a clear causal connection between β oscillations and the symptoms of Parkinson's disease still remains unclear (Kuhn *et al*., 2009; Weinberger *et al*., 2009), it has been shown that pathological oscillations are suppressed by volitional movement (Priori *et al*., 2002; Amirnovin *et al*., 2004), dopamine replacement therapy (Brown *et al*., 2001; Levy *et al*., 2002; Priori *et al*., 2004; Weinberger *et al*., 2006) and STN DBS in some studies, but not others (Foffani *et al*., 2006; Wingeier *et al*., 2006; Kuhn *et al*., 2008; Rossi *et al*., 2008). Furthermore, the degree of suppression of the β oscillations by dopamine therapy correlates with improvement of the hypokinetic symptoms of Parkinson's disease, namely akinesia/bradykinesia and rigidity, although not tremor (Kuhn *et al*., 2006, 2009; Ray *et al*., 2008).

β-oscillatory activity is seen largely within the dorsolateral portion of the STN (Kuhn *et al*., 2005; Weinberger *et al*., 2006; Trottenberg *et al*., 2007; Moran *et al*., 2008; Zaidel *et al*., 2009), the same location that seems to provide optimal therapeutic benefit to patients undergoing STN DBS (Herzog *et al*., 2004; Godinho *et al*., 2006; Maks *et al*., 2009). In addition, the sensorimotor region of the STN is primarily located dorsolaterally (Monakow *et al*., 1978; Nambu *et al*., 1996; Rodriguez-Oroz *et al*., 2001; Romanelli *et al*., 2005). It would therefore seem plausible to suggest (Trottenberg *et al*., 2007) that β-oscillatory activity may mark the sensorimotor region in the Parkinsonian STN, and that STN DBS outcome would be dependent on accurately targeting this region. In this manuscript we present support for this hypothesis by showing a strong correlation between the spatial extent of microelectrode recording β oscillations, the sensorimotor region of the STN and the therapeutic outcome of STN DBS. We further present an analysis of the characteristics and spatial distribution of periodic neural oscillations within the STN, and correlation thereof to the therapeutic response of Parkinson's disease symptoms to DBS and dopamine replacement medication.

Materials and methods

Patients and surgery

The microelectrode recordings from 128 patients with Parkinson's disease undergoing surgery for bilateral STN DBS were analysed in this study. Patients with prior pallidotomy ($n = 8$, not included in the 128) were excluded *a priori* due to concerns that their microelectrode recordings may not be representative of the Parkinson's disease STN (Mogilner *et al*., 2002; Zaidel *et al*., 2008). All patients met accepted selection criteria for STN DBS and signed informed consent for surgery with microelectrode recording. This study was authorized and approved by the Institutional Review Board of Hadassah University Hospital in accordance with the Declaration of Helsinki (reference codes: 0545-08-HMO and HMO:10-18.01.08).

Surgery was performed using the CRW stereotactic frame (Radionics, Burlington, MA, USA). STN target coordinates were chosen as a composite of indirect anterior commissure—posterior commissure atlas based location and direct (1.5 or 3 T) T_2 magnetic resonance imaging (MRI), using Framelink 4 or 5 software (Medtronic, Minneapolis, USA). All recordings used in this study were made while the patients were awake and not under sedation. The patient's level of awareness was continuously assessed clinically, and if drowsy the patient was stimulated and awoken, through conversation, by a member of the surgical team. Data were obtained off dopaminergic medications (>12 h since last medication) and during periods of rest or passive manipulation of the patient's limbs (somatosensory examination, see below).

Microelectrode recordings and recording stability inclusion criteria

Data were acquired with the MicroGuide system (AlphaOmega Engineering, Nazareth, Israel). Neurophysiological activity was recorded via polyamide coated tungsten microelectrodes (Alpha Omega) with impedance mean ± standard deviation (SD): 0.63 ± 0.16 MΩ (measured at 1 kHz at the beginning of each trajectory). The signal was amplified by 10 000 or 25 000, band-passed from 250 to 6000 Hz, using a hardware four-pole Butterworth filter, and sampled at 24 or 48 kHz by a 12-bit A/D converter (using ±5 V input range). One trajectory was mistakenly sampled at 12 kHz. Local field potentials were not recorded due to constraints of electrical noise in the operating room.

For both the left and right hemispheres, a microelectrode recording trajectory using one or two parallel microelectrodes was made, starting at 10 mm above the calculated target (centre of the dorsolateral STN). Our trajectories followed a double-oblique approach towards the dorsolateral STN target, designed to avoid the cortical sulci, the ventricles and major blood vessels (Machado *et al*., 2006). Therefore, although primarily in a dorsal-ventral direction, trajectories also took an anterior-posterior and lateral-medial course. A typical trajectory was ~60° from the axial anterior commissure–posterior commissure plane and 15° from the mid-sagittal plane. For simplicity we speak about STN depth along the trajectory and about the dorsal (or dorsolateral) versus ventral (or ventromedial) regions of the trajectory. When two microelectrodes were used, a 'central' electrode was directed at the centre of the dorsolateral STN target (as per imaging), and an 'anterior' electrode was advanced 2 mm anterior to the central electrode (in the parasagittal plane). The anterior electrode therefore traversed the STN more anteriorly and also more ventrally than the central electrode (due to the double-oblique approach).

The electrodes were advanced in small discrete steps, towards the estimated centre of the dorsolateral STN. Step size (ranging 400 μm down to 50 μm) was controlled by the neurophysiologist in order to achieve optimal recording and identification of upper and lower borders of the STN. Typically shorter steps were used as the electrode was advanced closer to the presumed location of the STN. Step size within the STN was 96.5 ±27.8 μm (mean ± SD). Following a 2 s signal stabilization period after electrode movement cessation, multi-unit traces were recorded.

Conditions in the operating-room often result in non-stable recordings (e.g. due to further movement of brain tissue in relation to the electrode tip or due to neuronal injury). The data traces were therefore analysed for recording stability with custom software. This was done by dividing each data trace into consecutive segments of 50 ms and computing the root mean square (RMS) for each segment. A section of the trace was considered stable when all corresponding segments' RMS values lay within 3 SDs of the median RMS. The longest stable section of the data trace was then selected for further analysis, discarding the rest of the trace. This type of stability analysis rejects infrequent events such as glitches (spurious electronic signals caused by brief, unwanted surges of electric power) or cell injury but does not reject (>1 Hz) oscillatory activity. All stable sections within the STN were longer than 2 s (duration mean ± SD: 13 ± 11 s; $n = 18\,658$ STN recording locations). Only electrode trajectories that passed through the STN were used.

STN entry and exit were discerned visually by one of the authors (A.Z.) as a sharp increase and decrease, respectively, in the normalized root mean square (NRMS, see below) of the neuronal signal (Moran *et al*., 2006; Zaidel *et al*., 2008). Similarly, the boundary between the dorsolateral oscillatory region and ventral non-oscillatory region was discerned visually, by a sudden decrease in β oscillations (e.g. Figs 1B and 8B; Zaidel *et al*., 2009). In order to avoid possible bias, these boundaries were also determined automatically using a hidden Markov model (Zaidel *et al*., 2009) and results compared.

A total of 314 microelectrode trajectories (taken from 128 patients with Parkinson's disease) were used in this study (Fig. 3A, top plot). All 314 trajectories had a clearly defined STN-entry and 272 had a clearly defined STN-exit (for the remainder, recording was stopped before exiting the STN). Therefore n = 272 in Fig. 1A and Supplementary Fig. 1, where STN-exit was required in order to normalize by STN length. All 314 trajectories traversed >3 mm of STN (94% traversed >4 mm of STN), with a mean STN recording span of 5.7 ± 1.1 mm (mean ± SD). The dorsolateral oscillatory region-ventral boundary was clearly discernable in 249 of the 314 microelectrode trajectories (79.3%), and 91% of patients had at least one discernable dorsolateral oscillatory region. All microelectrode recordings within the STN were then divided into dorsal and ventral regions, by the dorsolateral oscillatory region boundary (for the 249 trajectories with a clear dorsolateral oscillatory region boundary), or by the midpoint between STN-entry and -exit (for trajectories with no discernable dorsolateral oscillatory region boundary). Twelve trajectories were lacking both a clear dorsolateral oscillatory region boundary and STN-exit so this

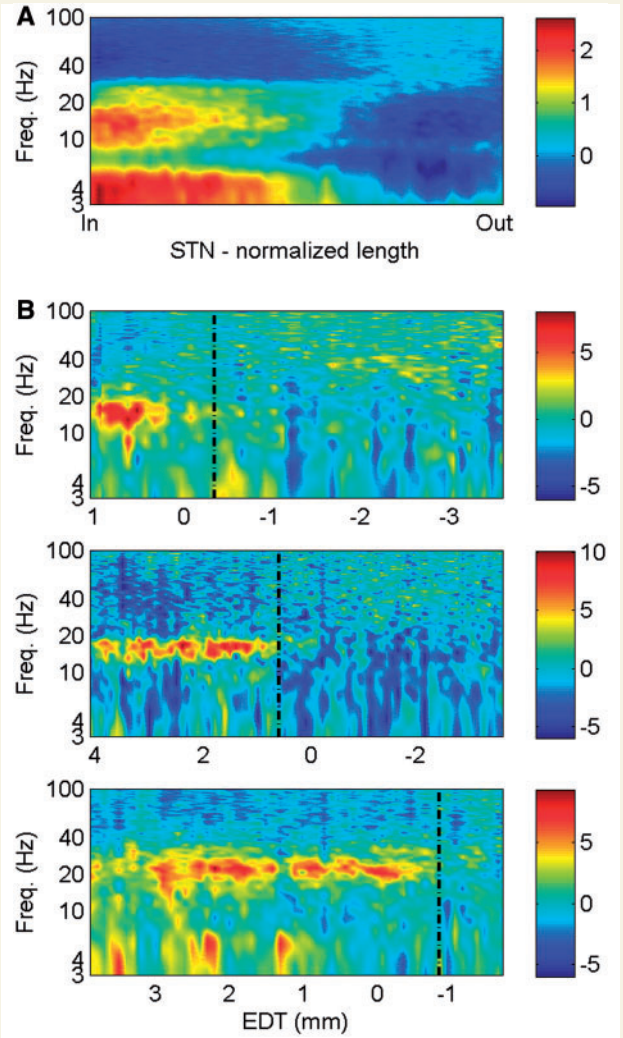

Figure 1 A distinct β-oscillatory region in the dorsolateral STN. (**A**) The mean power spectral density of the STN ($n = 272$ electrode trajectories) demonstrates increased β oscillatory activity in the dorsal STN. Trajectories were normalized by STN length. (**B**) The STN power spectral density plots of three example trajectories (from three patients); each present a distinct dorsolateral oscillatory region of different length. The black dot–dash vertical lines indicate the ventral boundary of the dorsolateral oscillatory region. The left and right extremities of the plot represent the dorsal (in) and ventral (out) boundaries of the STN, with absolute values (mm) marked on the abscissa. The colour-scale represents $10 \log_{10}$ (power spectral density power/average power spectral density power). EDT = estimated distance to target (defined as STN centre according to preoperative imaging).

division could not be made, and four trajectories did not have ventral recordings (the dorsolateral oscillatory region traversed the whole STN). This resulted in $n = 302$ and 298 for dorsal and ventral analyses, respectively (Fig. 3A–C).

The root mean square and impedance normalization

The RMS estimate of the raw multi-unit activity recorded by the microelectrode at each electrode depth was defined as follows:

$$\mathrm{RMS}(\bar{X}) = \sqrt{\frac{\sum_{i=1}^{n}(X_i - \mu)^2}{n-1}}, \quad (1)$$

where $\bar{X}$ is the vector of the sampled analogue signal with mean μ, X_i is each sample and n is the number of samples in the segment. RMS values are susceptible to electrode properties (e.g. electrode impedance); hence the RMS required normalization in order to be an absolute measure. As in previous studies, we normalized the RMS by the pre-STN (white matter) baseline RMS (Moran *et al*., 2006; Zaidel *et al*., 2008, 2009), creating what we termed the NRMS. This method has been very useful in detecting STN borders and for displaying the microelectrode recording trajectory graphically (e.g. Fig. 8A).

In this study, we wanted to compare the mean-RMS in the STN to clinical parameters, such as symptom severity and postoperative improvement. This prompted our reassessment of the normalization method. It was seen that despite baseline normalization, the STN NRMS still demonstrated significant correlation to electrode impedance (measured at 1 kHz at the beginning of each trajectory; $R = -0.32$, $P < 0.0001$; Supplementary Fig. 4A). The correlation coefficient indicates that 10% (R^2) of mean NRMS variability in the STN could be explained by electrode impedance. This confounding effect could mask underlying clinical correlations. We therefore employed an alternative method for normalizing RMS in the STN: impedance-normalized RMS (INRMS). The INRMS in the STN was calculated by the following formula:

$$\mathrm{INRMS}_i = \mathrm{RMS}_i - a \times \left[I_i - \mathrm{mean}(\bar{I})\right], \quad (2)$$

where RMS_i is the mean RMS within a particular STN in microvolts and I_i is the corresponding electrode impedance in mega-ohms (MΩ measured at 1 kHz). $\bar{I}$ is the vector of all impedances, a is the linear coefficient of the regression line between the RMS vector and $\bar{I}$ (−6.9 in our data). The first factor subtracted from RMS_i, $a \times I_i$, corrects the linear dependence on impedance, whilst the second factor, $a \times \mathrm{mean}(\bar{I})$, ensures that after impedance normalization, the mean is unchanged in relation to the *raw*, unnormalized RMS (NRMS has a different mean).

We found that the mean normalized RMS (NRMS, normalized by pre-STN baseline activity) did not correlate significantly with Parkinson's disease symptoms or postoperative improvement (Supplementary Fig. 4C and E). Normalizing the RMS by impedance removed the confounding impedance correlation (Supplementary Fig. 4B) and revealed a significant correlation with both preoperative rigidity and postoperative reduction in Unified Parkinson's Disease Rating Scale (UPDRS) (Supplementary Fig. 4D and F, respectively). This same impedance normalization method was used to normalize the power spectral density (see below).

The power spectral density

For power spectral density calculations, the raw analogue signal was rectified by the 'absolute' operator and the mean was subtracted (Moran *et al*., 2008; Moran and Bar-Gad, 2010). Using the rectified signal, which follows the envelope of multi-unit activity, we were therefore able to detect burst frequencies below the range of the operating room band-pass filter (250–6000 Hz). Since the local field potential frequency domain was filtered out by the recording apparatus, our resulting power spectral density represents only spiking activity. The average power spectral density was calculated in each trace using Welch's method, with a 1 s Hamming window (50% overlap) and spectral resolution of 1/3 Hz. Values within 2 Hz of the 50 Hz power supply artefacts and their harmonics were removed and interpolated from the surrounding values. Two different methods were used to normalize the power spectral density:

(i) Dividing the power spectral density by the total power of the signal between 3 and 200 Hz (excluding power spectral density values within 2 Hz of the 50 Hz power supply artefacts and their harmonics) creating a relative power spectral density. This method exposed the 'relative' power across frequencies. For example two pure sine waves with the same frequency but of different amplitudes would have identical relative power spectral densities. This method is particularly useful in identifying the dorsolateral oscillatory region of the STN (Zaidel *et al*., 2009). The relative power spectral density can be seen in Figs 1, 3, 4 and 8, and Supplementary Figs 1 and 5.

(ii) Normalizing the power spectral density by electrode impedance in the identical manner as the described above for the RMS (i.e. by offsetting its correlation with the measured electrode impedance). This method retained the 'absolute' level of power, exposing the magnitude for each frequency in the signal. In the above example of two sine waves with the same frequency but of different amplitudes (measured by equal impedance electrodes), the impedance normalized power spectral densities would be different. Since the dependence of power on electrode impedance could be different for specific power spectral density frequencies, the normalization was performed separately for each frequency band in question. In order to qualify this, we computed the correlations for 1–100 Hz power spectral density individually (in steps of 1 Hz)—all correlations were significant ($P < 0.01$; median $P < 0.0001$). Furthermore, re-analysis using a single value for normalization across all frequencies (the mean linear coefficient of the regression line) did not change our results presented below. This method was used for the regression analysis presented in Fig. 7.

For all power spectral density normalization, correlation analyses and plotting in this manuscript, the logarithm of the power spectral density was used.

Goniometers

In order to measure joint angle, two goniometers (Biometrics Ltd, UK) were attached to the patient's arm, contralateral to recording—one to the wrist and one to the elbow. Coban wrap (3M Health Care, MN) was used for fixation. One axis of movement (flexion and extension) was recorded for each joint. The goniometer signals were amplified, sampled at 3 kHz and fed into the MicroGuide data acquisition system (see above). Hence the neuronal and goniometer recordings were synchronized.

The patients' joints were moved passively one at a time by the neurosurgeon (whilst fixating the other joint to avoid biomechanically coupled movements). Only recording locations that had five or more repetitions of flexion and extension for both joints were used, resulting in 231 recordings from 50 trajectories (28 patients).

For 103 of the locations, the joints were moved at 0.5 and 1 Hz by the neurosurgeon, who was wearing a metronome headset for timing (the paced paradigm)—52 and 51 in the dorsolateral oscillatory region and ventral STN, respectively. The remaining recordings entailed the same type of repetitive movement, but self-paced by the neurosurgeon without a metronome (generally at a single frequency between 0.5 and 1 Hz). Below, we present the results from the paced subset; however, responses across the whole dataset were very similar.

The moving RMS of the neuronal signal was calculated with a Gaussian window (window size = 120 ms) and with 1 ms step resolution. Each signal was inspected by one of the authors (A.Z.), and if a recording artefact was discerned, it was marked for exclusion (see below). Flexion and extension were detected automatically from the recorded goniometer signal by its derivative crossing an empirical threshold (with hysteresis to prevent double detection). The peristimulus time histogram of the RMS was calculated around each detection, comprising 250 ms before and 500 ms after the detection. If an artefact was marked within half the Gaussian window size (60 ms) from the edges of the peristimulus time histogram, the detection was rejected.

The threshold for detection of a neural response to passive manipulation of the limbs was generated for each type of detection (wrist/elbow; flexion/extension 0.5/1 Hz) by a resampling (bootstrap) method, as follows: between the first and last detection, random points were generated in accordance with the number of detections. For example, if there were 20 wrist flexion detections at 0.5 Hz, 20 random points were generated between the first and the last detection. The SD of the RMS-peristimulus time histogram around the random points was then extracted. This was repeated 100 times, and the average SD was computed. A somatosensory response was deemed significant if the real RMS-peristimulus time histogram deviated from its mean by 3 (averaged) SDs. For the paced paradigm, a joint was considered responsive if it responded at both frequencies.

Clinical data

In this study we correlated clinical data with the intraoperative microelectrode physiological recordings. For these correlations, only recordings from the macroelectrode implanted trajectories were used, *a priori*. These recordings were assumed to represent the region stimulated postoperatively best and to represent the patient's underlying STN pathophysiology. Electrophysiological measures were then averaged between the two hemispheres to obtain a single value per patient for comparison to clinical data.

However, only a subset of the patients with full electrophysiological data had preoperative clinical data, and only a subset of this group also had postoperative clinical data. This restricted the number of patients (n) for any given analysis to those patients with the complete, necessary dataset. To support the claim that patient subsets were representative of the whole, the power spectral density analysis was re-run using only the subset of patients for which postoperative clinical improvement could be calculated (Supplementary Fig. 5). No significant differences were seen between this subset and the rest of the data. The number of patients used for the clinical comparisons are detailed below.

We used the third subsection of the UPDRS-III (UPDRS-III, motor score breakdown; max = 108; Fahn *et al*., 1987) in order to quantify the clinical state of the patient and clinical response to treatment. The UPDRS-III was broken into four composite symptom scores as follows:

(i) tremor: sections 20–21 (max 28),
(ii) rigidity: section 22 (max 20),
(iii) limb-bradykinesia: sections 23–26 (max 32),
(iv) axial-bradykinesia: sections 18–19 and 27–31 (max 28).

For many of the patients analysed in this study ($n = 103$) the preoperative UPDRS-III score, both off and on antiparkinsonian medication (PRE-OFF and PRE-ON, respectively), was available. For 82 of these 103 patients, the symptom breakdown scores were available; for the remaining 21 only the total score was available. In the multiple regression analysis between the preoperative scores and specific oscillation frequencies (Fig. 7A), $n = 86$ and 71 for the total and symptom breakdown comparisons, respectively, due to missing impedance values (required to normalize the power spectral density).

For a subset of the patients with preoperative UPDRS-III scores, postoperative UPDRS-III scores were also available. Postoperative UPDRS-III was assessed in four scenarios: (i) off medication, off stimulation; (ii) off medication, on stimulation; (iii) on medication, off stimulation; and (iv) on medication, on stimulation (POST-OFF, POST-STIM, POST-ON and POST-BOTH, respectively). Patients were off medications for $>$ 12 h for PRE-OFF, POST-OFF and POST-STIM testing, and off stimulation for $>$0.5 h for POST-OFF and POST-ON testing. Postoperative testing was 16 ± 8 months (median ± median absolute deviation) after surgery. Postoperative percentage improvement was calculated for n = 45 patients as follows:

$$100 \times \frac{\text{POST-OFF} - X}{\text{POST-OFF}} \quad (3)$$

replacing X by POST-ON, POST-STIM or POST-BOTH ($n = 31$, 45 and 44, respectively, due to missing scores). For symptom specific improvement: $n = 29$, 43 and 42, respectively, due to missing breakdown scores for two patients. In the multiple regression analysis between postoperative improvement and specific oscillation frequencies (Fig. 7B–D), $n = 29$, 41 and 40, respectively, for total UPDRS-III comparisons and $n = 27$, 39 and 38, respectively, for symptom breakdown comparisons (due to missing impedance values).

The power spectral density analysis was rerun for the 45 patients for whom we could calculate postoperative improvement. Supplementary Fig. 5 demonstrates that they are a representative sample of the larger population used in this study. In correlating postoperative improvement with dorsolateral oscillatory region length (Fig. 2 and Supplementary Fig. 2), three of the patients with the required clinical data did not have a discernable dorsolateral oscillatory region boundary, hence $n = 42$ and 41 for POST-STIM and POST-BOTH, respectively. Of these patients, STN exit was missing for one, hence $n = 40$ (POST-BOTH) in Supplementary Fig. 3 where STN length was also required.

Postoperative optimization of deep brain stimulation parameters

Postoperatively, stimulation parameters such as pulse frequency, width and amplitude, as well as which contact(s) to activate were chosen by the neurologist for optimal clinical benefit. This was done without access to microelectrode recording data. Hence the choice of contact location was clinical in nature. The centre of stimulation was deduced as the midpoint of the active (cathode, negative) contact(s) in relation to the STN (Lujan *et al*., 2009). For >95% of the cases, stimulation was either monopolar or 'bimonopolar' (i.e. two contacts with the same negative polarity were used). When an additional contact was used for dyskinesia management (generally one of the two top contacts, dorsal to the STN; Herzog *et al*., 2007) it was not included as an active contact. Alignment between the macroelectrode and microelectrode recording recordings was accomplished by

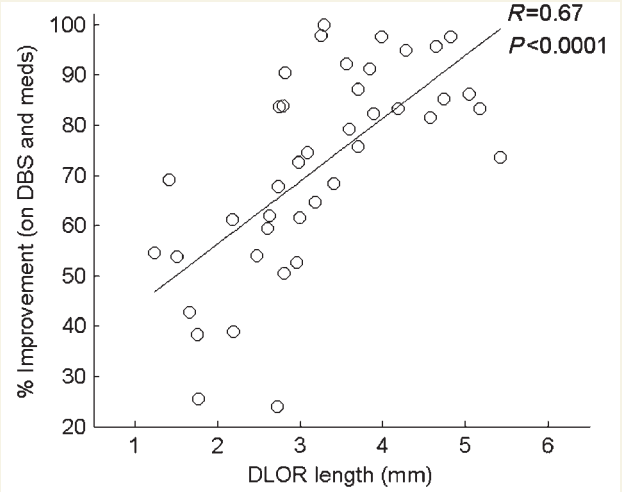

Figure 2 The spatial extent of STN β oscillations predicts the outcome of STN DBS. A strong correlation is seen between the postoperative percent improvement due to stimulation and medication, and the length of the dorsolateral oscillatory region (DLOR, mean DLOR-length of the implanted trajectories from both hemispheres). Percentage improvement = total UPDRS III (POST-OFF−POST-BOTH)/POST-OFF; $n = 41$ patients.

overlaying the macroelectrode contacts on the microelectrode recording trajectory (Fig. 8A) with the base of the second contact (counting bottom-up) at the midpoint between the defined STN borders—in the identical manner to macroelectrode placement during surgery.

Statistical analysis

For correlation analyses, the correlation coefficient is represented by the letter *R*. The corresponding probability value (*P*) is the probability of getting *R* as large as the observed value by random chance when the true correlation is zero, and was computed by transforming the correlation to create a *t*-statistic. When there were multiple comparisons, the Bonferroni correction was used (i.e. the obtained *P*-value was multiplied by the number of comparisons) before significance testing ($P < 0.05$).

Software

Data analysis was carried out on custom software using MATLAB V7.1 (Mathworks, Natick, MA).

Results

A distinct region of β oscillations in the subthalamic nucleus

Power spectral density was calculated across the STN depth (primarily in a dorsolateral–ventromedial direction, see methods). Plotting a spectrogram-by-depth (averaged across electrode trajectories that traversed and exited the STN, $n = 272$), demonstrates that β-oscillatory activity lies predominantly in the dorsolateral region (Fig. 1A and Supplementary Fig. 1). This is in accordance with other local field potential (Kuhn *et al*., 2005; Weinberger *et al*., 2006; Trottenberg *et al*., 2007) and single unit (Moran *et al*., 2008) studies, which, like Fig. 1A, have described the dorsolateral spatial location of β oscillations by pooling data across patients. The pooled data presents a gradient of β-oscillatory activity (more oscillations dorsally, less ventrally) giving the impression of a continuum, as opposed to a distinct region of β oscillations.

Such a mean-gradient, however, does not necessitate that *each* individual trajectory has a gradient. Rather it can arise from the pooling of numerous trajectories, each of which have a *distinct* oscillatory/non-oscillatory boundary but at different depths. Inspection of individual spectrogram-by-depth plots indeed reveals that most trajectories have a distinct dorsolateral oscillatory region with a discernable ventral-boundary (as opposed to a gradient). Figure 1B presents three example trajectories, each displaying a distinct dorsolateral oscillatory region, but of diverse (short, medium and long) spatial expanse. The success of a hidden Markov model in detecting the dorsolateral oscillatory region of a microelectrode recording trajectory automatically (Zaidel *et al*., 2009) confirms the notion of a sharp boundary between the dorsolateral oscillatory region and ventral, non-oscillatory STN.

The extent of the dorsolateral oscillatory region predicts the outcome of subthalamic nucleus deep brain stimulation

A striking correlation was seen between the outcome of STN DBS, calculated as the percentage improvement in the UPDRS-III score on stimulation and medication, and the length of the dorsolateral oscillatory region in the implanted trajectory ($R = 0.67$, $P < 0.0001$, Fig. 2). This was the result of dorsolateral oscillatory region length and not STN length, since the relative length of the dorsolateral oscillatory region within the STN (%) also correlated significantly with the outcome of STN DBS ($R = 0.47$, $P = 0.01$). Furthermore, running a multiple correlation (regression) analysis using both dorsolateral oscillatory region and STN length showed a significant correlation for dorsolateral oscillatory region length ($P = 0.001$) but not STN length ($P = 0.11$). When comparing improvement from DBS alone, OFF medication or when using the hidden Markov model method to detect the dorsolateral oscillatory region automatically (Zaidel *et al*., 2009) a strong correlation was still evident (Supplementary Fig. 2). All the significant *P*-values presented above are after the Bonferroni correction for multiple comparisons (the non-significant value presented was not corrected).

In order to increase our understanding of the correlation between postoperative UPDRS-III improvement and dorsolateral oscillatory region length, we broke the comparison down to the four composite symptom scores (tremor, rigidity, limb-bradykinesia and axial-bradykinesia). Our results demonstrated a significant correlation between absolute dorsolateral oscillatory region length and postoperative improvement of all symptoms apart from tremor (Supplementary Fig. 3). However, the lack of correlation with tremor improvement could be due to strong ceiling effects, since 71% of the patients had complete tremor improvement

postoperatively (in line with the consensus that tremor improvement on STN DBS is higher in comparison to other symptoms; Benabid *et al*., 2009).

Interestingly, the preoperative response to levodopa did not correlate with dorsolateral oscillatory region length ($P = 0.33$). This was also seen when testing only the subset of patients with postoperative scores ($P = 0.36$). Hence we conclude that the absolute dorsolateral oscillatory region length in the trajectory predicts the response of Parkinson's disease motor symptoms to STN DBS. This may reflect the surgeon's ability to find the largest (optimal) dorsolateral oscillatory region, or may indicate that DBS and levodopa work through different mechanisms. We will address this point later on.

Characteristics and spatial distribution of oscillations in the subthalamic nucleus

The mean power spectral density in the spiking activity of the STN demonstrates oscillatory activity with peaks at ~10, ~15 and ~25 Hz (Fig. 3A, top, blue plot). The mean power spectral density of the dorsolateral STN (Fig. 3A, middle, red plot) displays relatively increased β-oscillatory activity (13–30 Hz, with a maximal peak at ~15 Hz), and decreased high-frequency gamma activity (30–100 Hz). In contrast, the mean power spectral density in the remaining ventral STN (Fig. 3A, middle, green plot) displays relatively

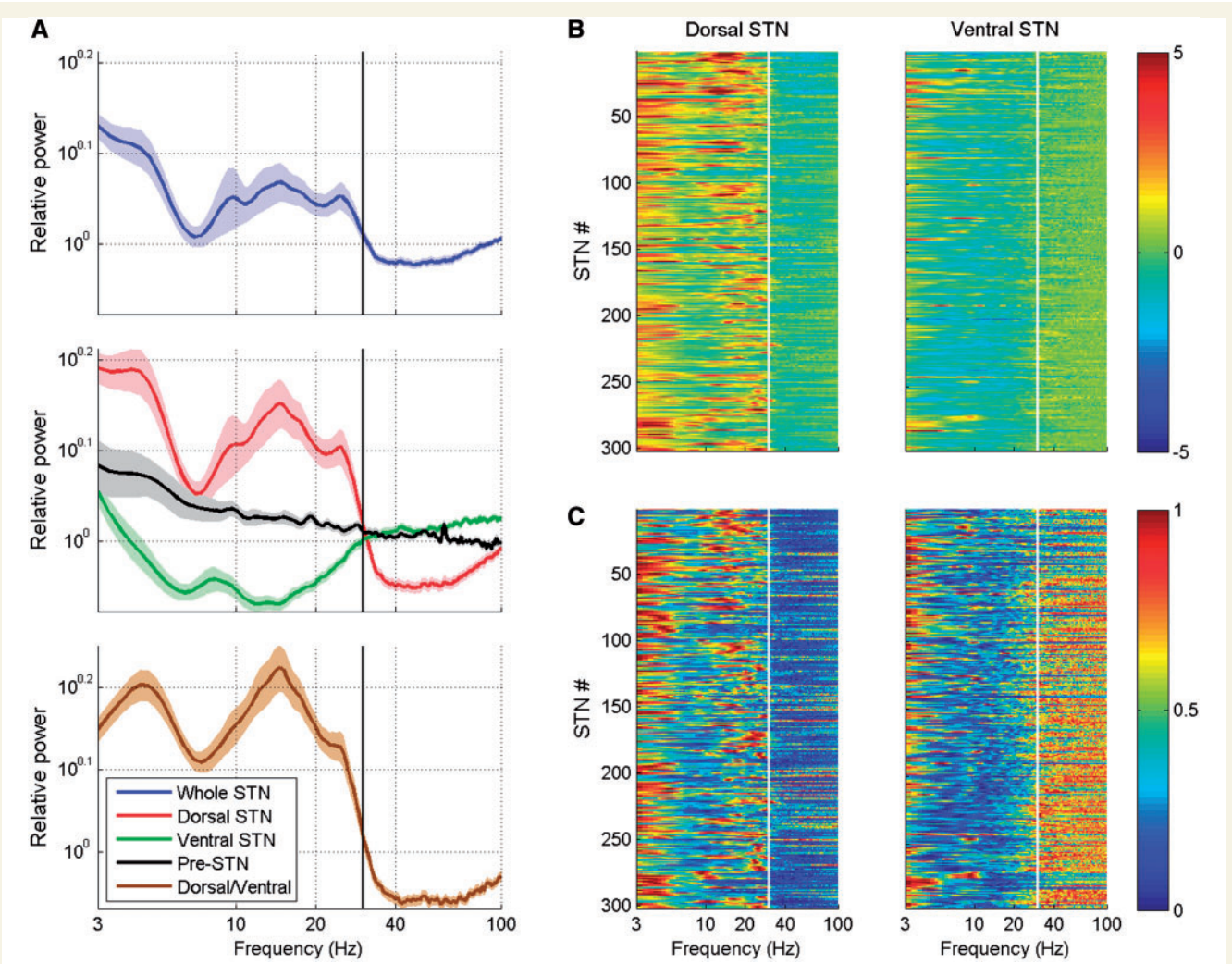

Figure 3 Dorsal β and low-frequency oscillations versus ventral gamma activity. (**A**) The mean relative power spectral density in the STN (blue), dorsal STN (red), ventral STN (green), prior entering the STN (pre-STN; black) and the difference between the dorsal and ventral STN (ratio presented in log scale; brown). The shaded regions mark the respective 95% confidence intervals. The dorsal STN demonstrates a peak in the β range whereas the ventral STN demonstrates increased gamma activity. The difference plot (brown) also demonstrates dorsal 5 Hz oscillations. (**B** and **C**) The mean relative power spectral densities in the dorsal (left column) and ventral (right column) subterritories of the STN demonstrate that most trajectories (STN #) can be divided into dorsal and ventral regions with increased 5 Hz and β oscillatory activity versus gamma activity, respectively. (**B**) The colour-scale represents $10 \log_{10}$ (power spectral density power/average power spectral density power), truncated above/below 5 and −5, respectively. (**C**) The same as **B**, but each trajectory was normalized to range between 0 and 1 (no truncation). A vertical line (black in **A**; white in **B** and **C**) is drawn at 30 Hz. $n = 314$ electrode trajectories from 128 patients. $n = 302$ and 298 for dorsal and ventral plots, respectively.

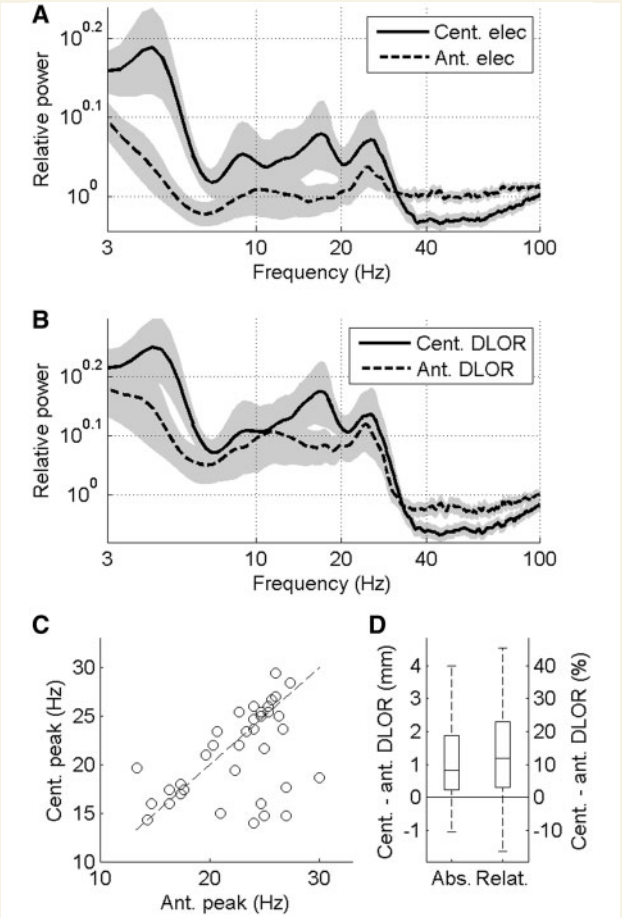

Figure 4 Different distribution of oscillation frequencies and their spatial extent in the central and anterior STN trajectories. (**A**) The mean relative power spectral density of the STN demonstrates more ~5 Hz and β oscillations recorded in the central (cent.) versus anterior (ant.) electrode trajectory. (**B**) The mean relative power spectral density of the dorsolateral oscillatory region (DLOR) demonstrates larger oscillatory peaks at ~5 and ~15 Hz centrally versus anteriorly. For **A** and **B**, the shaded regions mark the 95% confidence intervals. (**C**) The β frequency peak was often similar for the central and anterior electrode trajectories (points along the diagonal), and when dissimilar, the anterior electrode trajectory generally demonstrated a higher frequency peak than the central (points below the diagonal). The dashed line represents the diagonal $y = x$. (**D**) The difference between the central and anterior dorsolateral oscillatory region length (both absolute length and relative proportion of the trajectory's STN length, left and right box plots, respectively) demonstrates that the dorsolateral oscillatory region was significantly longer in the central versus anterior electrode trajectory ($P < 0.0001$ for both, after Bonferroni correction for multiple comparisons). The horizontal line represents $y = 0$ (equal dorsolateral oscillatory region lengths). For the box and whisker plots, the bottom and top of the box represent the lower and upper quartiles, respectively, and the band near the middle of the box represents the median. The whiskers show the minimum and maximum of all the data. $n = 71$ trajectories for **A**. A dorsolateral oscillatory region, a peak in β frequency or STN-exit was not detected for all trajectories. Hence for **B**, $n = 65$ and 50 for the central and anterior electrode trajectories, respectively, (**C**) $n = 37$ and (**D**) $n = 48$ and 41 for the absolute and relative lengths, respectively.

decreased β-oscillatory activity and increased gamma activity (see also Fig. 1A, and Supplementary Fig. 1A and B). This phenomenon is highly consistent across patients (Fig. 3B and C). The increased β activity, seen dorsally, is characterized by high variance and is often marked by peaks at various frequencies (for different patients) within the β range (Weinberger *et al*., 2006; Kuhn *et al*., 2009). In contrast, the gamma activity, seen primarily ventrally, is characterized by low variance without sharp frequency peaks. This can also be discerned by the SD and median absolute deviation plots, presented in Supplementary Fig. 1C and D, respectively.

Although our current analysis focuses mainly on the β-frequency range, low-frequency activity (around the approximate tremor frequency, ~5 Hz) as well as ~10 Hz activity were also seen, albeit less consistently, in the STN (Bergman *et al*., 1994; Moran *et al*., 2008; Amtage *et al*., 2009; Reck *et al*., 2009). The low-frequency activity appeared mainly in the dorsolateral oscillatory region (Fig. 3A bottom, brown plot); however, when present, it did not define a continuous region as the β oscillations did (Fig. 1B, bottom plot). In contrast, ~10 Hz oscillations could be seen anywhere in the STN (Magill *et al*., 2006; Fig. 1A and Supplementary Fig. 1C).

For passes in which both electrodes traversed the STN (each for a minimum of 4 mm, $n = 71$ passes), a paired comparison between the central and anterior electrode trajectories could be made. Of the 71 passes, 65 presented a discernable dorsolateral oscillatory region in the central electrode trajectory versus 50 on the anterior. In addition, when a dorsolateral oscillatory region was discerned in both electrode trajectories, the central electrode dorsolateral oscillatory region was generally longer than the dorsolateral oscillatory region of the anterior electrode (Fig. 4D), both in absolute (mm) and relative (percentage within the STN recorded on that electrode) terms. This was probably due to the fact that the anterior electrode trajectory was also more ventral.

The central electrode trajectory demonstrated relatively higher β-oscillatory (and lower gamma) activity compared to the anterior (Fig. 4A). Comparing the power spectral density in the dorsolateral oscillatory region of the central versus anterior electrode trajectory demonstrated that ~5 and ~15 Hz β power occurred predominantly in the central versus anterior dorsolateral oscillatory region; however, higher frequency β power (~25 Hz) seemed to occur in both (Fig. 4B). The frequency value at the peak within the β range (13–30 Hz) was often similar for the central and anterior electrode trajectories. However, there were many STNs that demonstrated a low-β peak (~15 Hz) in the central electrode trajectory and a high-β peak (~25 Hz) in the anterior electrode trajectory (Fig. 4C). This does not imply that there was more ~25 Hz activity in the anterior electrode trajectory (in fact there was less, Fig. 4A), rather, there was considerably less ~15 Hz activity, thereby exposing the ~25 Hz peak. Hence, ~15 Hz activity was primarily observed in the central (maybe also more dorsal) region of the dorsolateral oscillatory region, whereas ~25 Hz seems to be in both the anterior and more central regions of the dorsolateral oscillatory region.

In conjunction with the observed differences in frequency distribution between the dorsolateral oscillatory region and ventral STN, and between the central and anterior electrode trajectories, there were also significant differences in the intensity

of the STN spiking activity. Impedance-normalized RMS (see Methods section) was larger in the dorsolateral oscillatory region versus ventral STN (mean ± SD = 12.9 ± 2.9 and 11. 9 ± 2.3 μV, respectively, $P < 0.0001$) and larger in the central versus anterior electrode trajectories (13.2 ± 2.7 and 11.8 ± 2.0 μV, respectively, $P < 0.0001$).

The subthalamic nucleus dorsolateral oscillatory region has increased somatosensory responses

Neuronal responses within the STN to passive movement of the contralateral limbs are generally tested during surgery subjectively (by listening for modulation of the audio output of the electrode signal; Hutchison *et al*., 1998; Rodriguez-Oroz *et al*., 2001; Theodosopoulos *et al*., 2003). In this study we added a quantitative computerized analysis of the STN somatosensory responses. For this purpose, elbow and wrist joint angles were monitored by two goniometers, recorded simultaneously with the neural activity. Figure 5A shows an example of the goniometer and microelectrode recordings. Flexion and extension movements were detected automatically and the peristimulus time histograms of the STN spiking activity were calculated for both joints (Fig. 5B). For the example in Fig. 5, a significant decrease in STN activity was detected in response to wrist extension, whereas a significant increase was detected for wrist flexion and elbow extension and flexion.

The spatial distribution of somatosensory responses across the STN is presented in Fig. 6A. Of the locations tested in the dorsolateral oscillatory region, 62% demonstrated responses to passive joint movement versus 25% in the ventral region ($P < 0.01$, after Bonferroni correction). This ratio (dorsolateral oscillatory region versus ventral percent responses) was similar in both the anterior and central electrode trajectories (Fig. 6B). However, on the whole, there was a higher ratio of responses in the central (versus anterior) electrode trajectory (Fig. 6C). This is in agreement with the larger spatial extent of the dorsolateral oscillatory region in the central electrode trajectory (Fig. 4D). The number of wrist responses was similar for the anterior and central electrode trajectories. In contrast, elbow responses were more prevalent in the central electrode trajectory (Fig. 6C; $P < 0.01$, after Bonferroni correction). In the central electrode trajectory, many STN sites responded to movement of both joints. This was not observed in the anterior electrode trajectory (Fig. 6C).

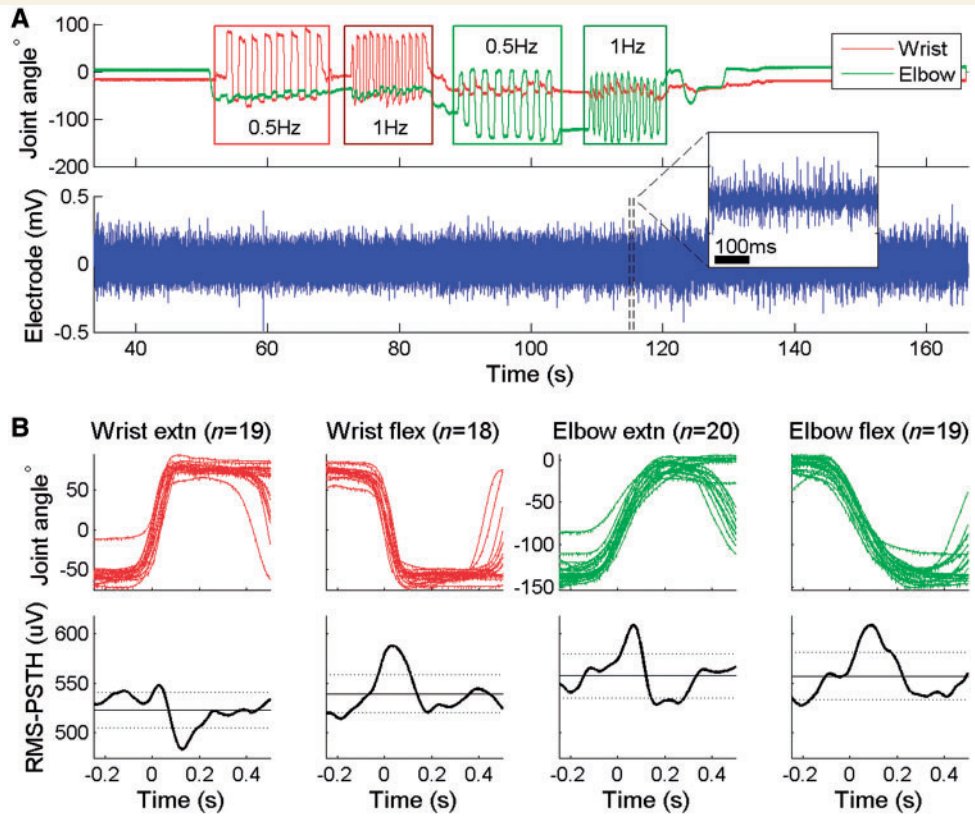

Figure 5 An example recording of STN neural activity during passive movement of a patient's arm showing somatosensory neuronal responses. (**A**) The wrist and elbow joint angles were monitored by goniometers (upper trace), simultaneous to multi-unit microelectrode recording from the contralateral STN (lower trace). The inserted plot is an arbitrary microelectrode recording section (marked by the vertical dashed lines) magnified in time. (**B**) Flexion and extension automatic detection, as well as the corresponding peri-stimulus time histogram (PSTH) of the microelectrode recording RMS, are presented for both joints. The horizontal solid lines indicate the mean peristimulus time histogram RMS, and the horizontal dotted lines indicate 3 SDs above/below.

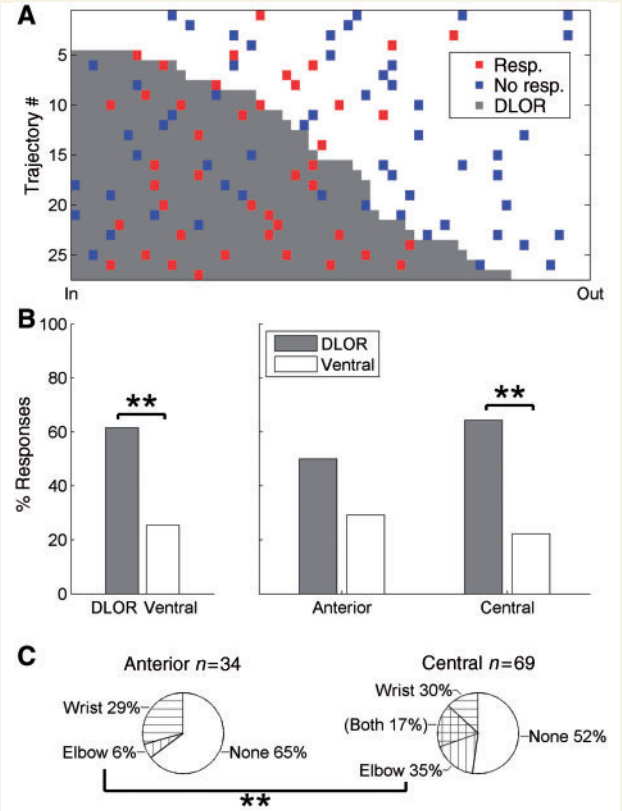

Figure 6 The dorsolateral oscillatory region (DLOR) and central electrode trajectory demonstrated a higher ratio of significant somatosensory responses. (**A**) The distribution of recording locations tested for somatosensory responses across STN trajectories, arranged by increasing dorsolateral oscillatory region proportion and normalized by STN length (with 59 steps, as per the mean number of recording locations within the STN). (**B**) The dorsolateral oscillatory region had a significantly higher percentage of somatosensory responses compared to the ventral region. The same was seen after sorting recordings by anterior and central electrode trajectories; however significance remained only for the central electrode trajectory. (**C**) Overall (without dividing into dorsolateral oscillatory and ventral region) the central electrode trajectory displayed a higher response ratio in comparison to the anterior. Wrist responses were similar for both electrode trajectories; however elbow responses were significantly more prevalent in the central. In **B** and **C**, $n = 103$ recording locations from 28 trajectories; in **A** one trajectory could not be used due to a missing STN-out score. $^{**}P < 0.01$ after Bonferroni correction for multiple comparisons.

Subthalamic nucleus oscillation frequencies predict individual motor symptom improvement

We have shown above that the clinical response to STN DBS correlates with the spatial extent of the dorsolateral oscillatory region. To further our understanding of the relationship between improvement of Parkinson's disease symptoms and STN oscillations, and to differentiate between specific frequency-bands, we compared the patient's response to the mean (impedance normalized) power spectral density, recorded in the implanted trajectory. As above, we used the total UPDRS-III score as well as the four composite symptom scores (tremor, rigidity, limb-bradykinesia and axial-bradykinesia). We compared symptom improvement to the low frequency (3–7 Hz) and β (13–30 Hz) oscillatory peak power (since oscillatory activity in these two bands was particular to the dorsolateral oscillatory region; Fig. 3A, bottom, brown plot). In order to do this, we ran a multiple regression, which gives the influence of each band on the outcome while taking into account the influence of the other.

We found that preoperative improvement from levodopa was consistently, although not significantly, associated with both low frequency and β oscillations. In particular, a good response to levodopa seemed to be predicted by 'increased' β, and 'decreased' low-frequency oscillations (Fig. 7A). Postoperatively, we saw a similar relationship between levodopa improvement and β oscillations, however, we did not observe a negative correlation with low-frequency oscillations (Fig. 7B–D). A significant correlation was seen (after the Bonferroni correction) between β-oscillatory activity and improvement in the total UPDRS-III score, as well as axial-bradykinesia and rigidity subscores, on STN DBS and medication (Fig. 7D). β oscillations tended to associate levodopa with improvement of limb-bradykinesia, and DBS with improvement in axial-bradykinesia (Fig. 7B and C, respectively). This was in line with another, similar observation: on DBS alone, improvement in axial (but not limb) bradykinesia correlated significantly with dorsolateral oscillatory region length; however, on DBS and medication, limb-bradykinesia also correlated significantly.

We were interested to see whether breaking down the β band further would associate specific oscillation frequencies with improvement on DBS versus levodopa. In order to avoid biases, we ran a multiple correlation between the mean (impedance normalized) power spectral density at five equidistant frequencies (5, 10, 15, 20 and 25 Hz—each calculated with a 4 Hz Gaussian window) versus symptom response to DBS and/or medication. We found that ~25 Hz oscillations were significantly associated with DBS (for axial-bradykinesia improvement), whereas ~15 Hz tended to correlate with the improvement (of rigidity) in response to medication. Although the latter was not significant after Bonferroni correction, it was seen for both the pre and postoperative responses to medication. Also, it was seen postoperatively on DBS and medication, but not on DBS alone (without medication).

The optimized electrode contact lies within the STN dorsolateral oscillatory region

During surgery, a DBS lead comprising four 1.5 mm macroelectrode contacts, separated by 1.5 mm (model 3387, Medtronic, MN, USA) was permanently implanted in the STN, such that the base of the second contact (counting bottom-up) coincided with the centre of the STN. Following surgery, the neurologist optimized stimulation parameters such as pulse frequency, width and amplitude, as well as which contact(s) to activate. We compared the site of optimal stimulation to the location of the

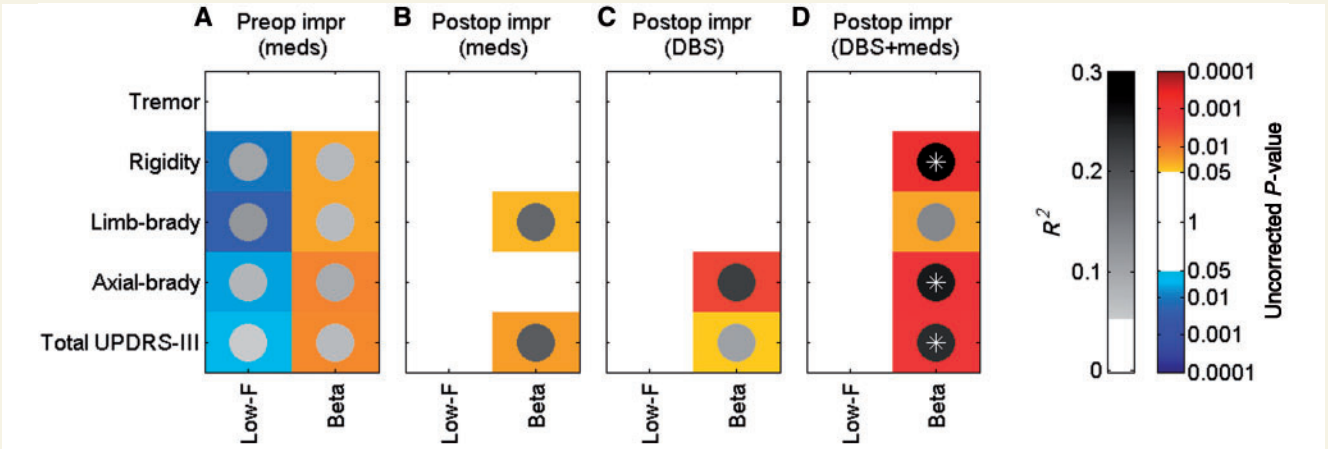

Figure 7 Postoperative clinical improvement on DBS and medication correlates significantly with the β power recorded in the macroelectrode implanted trajectory. Multiple regression analysis was run between a two-value vector comprising of low-frequency (Low-F, 3–7 Hz) and β (13–30 Hz) peak power (presented on the abscissa) versus improvement in the total and breakdown UPDRS-III scores (presented on the ordinate). Greyscale circles and coloured blocks represent the R^2 and corresponding *P*-values, respectively. Positive and negative correlations are represented by warm and cold coloured blocks, respectively. Only correlations with $P < 0.05$ (uncorrected) were plotted. Correlations which remained significant after Bonferroni correction for multiple comparisons were marked by an asterisk. (**A**) The preoperative response to levodopa tended to correlate positively with β power and negatively with low-frequency power. Although not significant after the Bonferroni correction, this was consistent across rigidity and axial/limb-bradykinesia subscores as well as the total UPDRS-III. When correlating postoperative improvement with β power, (**B**) medication and (**C**) DBS tended to be associated with limb and axial-bradykinesia subscores, respectively. Both showed a similar trend for the total UPDRS-III score. (**D**) Postoperative response on both DBS and medication correlated significantly with β power for rigidity and axial-bradykinesia subscores as well as for the total UPDRS-III score. A similar trend was seen for the limb-bradykinesia subscore. In **A**, $n = 86$ for the total and $n = 70$ for the symptom breakdown comparisons due to 16 missing symptom breakdown scores. In **B–D**, $n = 29$, 41 and 40, respectively, for total UPDRS-III comparisons. Of these, two patients were missing postoperative symptom breakdown scores. Pre- and postoperatively, tremor improvement could not be calculated for four and five patients, respectively, due to baseline tremor score = 0.

dorsolateral oscillatory region in the intraoperative microelectrode recording trajectory. A possible limitation of this comparison, is that being aware of the implantation procedure, the neurologist may have had a bias to the second or more dorsal contacts. Nonetheless, the active contact was selected without access to the individual patients' microelectrode recording results and was different across patients (spanned all four contacts). Hence coincidence of the selected contact and the dorsolateral oscillatory region centre would provide further support for the clinical importance of the dorsolateral oscillatory region.

The NRMS and power spectral density of an example trajectory are presented in Fig. 8A and B, respectively, with the four macroelectrode contacts of the implanted lead overlaid on the NRMS plot. The active macroelectrode contact (coloured in red) seems to lie well within the dorsolateral oscillatory region of the implanted trajectory. Across the population there was a high concurrence between the centre of stimulation (Lujan *et al.*, 2009) and the dorsolateral oscillatory region. The mean distance from the centre of stimulation to the centre of the dorsolateral oscillatory region was 0.36 ± 1.52 mm (mean ± SD, Fig. 8C). In contrast 1.79 ± 1.56 mm was measured to the centre of the STN ($n = 52$ trajectories). The null hypothesis of zero mean was tested for both measurements: it could not be rejected for the distance from dorsolateral oscillatory region centre ($P = 0.10$), but was strongly rejected for the distance from STN centre ($P < 0.0001$).

Discussion

In this article we have described the existence of a distinct dorsolateral oscillatory region in the STN of patients with Parkinson's disease as revealed by microelectrode recording of spiking activity. We have demonstrated that the length of the dorsolateral oscillatory region in the implanted trajectory correlates significantly with the outcome of STN DBS. This was seen for improvement in the total UPDRS-III motor score as well as symptom breakdown scores. The proximity of the active electrode contact, selected by the neurologist, to the centre of the dorsolateral oscillatory region is further support for the clinical importance of the dorsolateral oscillatory region. Hence, we conclude that dorsolateral oscillatory region length in the implanted trajectory predicts the response of Parkinson's disease motor symptoms to STN DBS.

Although dorsolateral oscillatory region length is partially dependant on surgical trajectory (the dorsolateral oscillatory region was significantly longer on the central versus anterior electrode trajectory and would be non-existent for trajectories that miss the STN), it is probably also dependant on patient physiology (e.g. a healthy patient would not have STN oscillatory activity; Wichmann *et al.*, 1994; Steigerwald *et al.*, 2008). We tested an association between the dorsolateral oscillatory region length and baseline Parkinson's disease symptoms (PRE-OFF), but our results were not conclusive. Hence, further investigation (including additional factors, e.g. the severity and distribution of dopamine

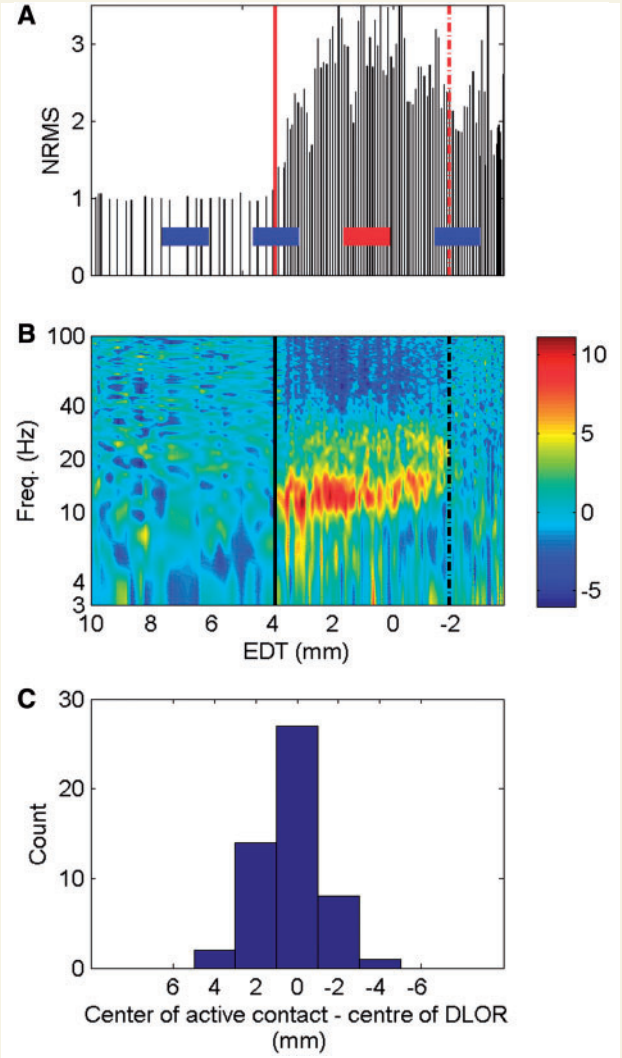

Figure 8 The clinically chosen (active) DBS contact coincides with the dorsolateral oscillatory region centre (DLOR). (**A**) The NRMS and (**B**) power spectral density of an example trajectory as a function of estimated distance to target (EDT). The power spectral density colour-scale represents $10 \log_{10}$ (power spectral density power/average power spectral density power). The red (**A**) and black (**B**) solid and dashed vertical lines indicate STN entry and the ventral boundary of the dorsolateral oscillatory region, respectively. The implanted macroelectrode's contacts are superimposed on the NRMS plot in **A** with the active contact, chosen by the neurologist to optimize clinical outcome, in red. (**C**) A histogram of the distance between the centre of the active macroelectrode contact and the centre of the dorsolateral oscillatory region.

depletion) is required. We suggest that dorsolateral oscillatory region length is a result both of surgical trajectory and patient pathophysiology, and reflects the potential for improvement by STN DBS. Therefore, accurate placement of the macroelectrode within the dorsolateral oscillatory region could lead to a better outcome for DBS surgery.

The dorsolateral oscillatory region is characterized by a continuous region of increased β oscillatory activity (13–30 Hz) and reduced gamma activity (30–100 Hz). In contrast, the ventral region of the STN demonstrates reduced β and increased gamma activity. Low-frequency (3–7 Hz) activity appeared mainly in the dorsolateral oscillatory region, however, it did not define a continuous region as β oscillations did. One may have thought that neurons in the dorsolateral oscillatory region may be entrained to oscillations and therefore not demonstrate responsiveness to external passive movement of the arm, or that the oscillations may obscure somatosensory responses. Rather, despite oscillations, significantly higher somatosensory responsiveness was found in the dorsolateral oscillatory region versus the more ventral, non-oscillatory region. This is in line with previous studies that have described the dorsolateral STN as the somatosensory region (Monakow *et al*., 1978; Nambu *et al*., 1996; Rodriguez-Oroz *et al*., 2001; Romanelli *et al*., 2005).

Increased somatosensory responsiveness in the dorsolateral oscillatory region leads one to believe that the dorsolateral oscillatory region overlaps the somatosensory region of the STN. However, complete congruency of the dorsolateral oscillatory region with the somatosensory STN seems improbable due to the broad range of dorsolateral oscillatory region lengths we encountered (ranging from none, to completely covering the STN). Furthermore, although to a lesser degree, somatosensory responses were also found in the non-oscillatory STN. Hence we propose that the dorsolateral oscillatory region marks a pathological region within the STN, which could span part of, or the whole of, the somatosensory region (and possibly even beyond).

Our finding that clinical improvement on DBS and medication significantly correlates with β power in the STN is in line with previous studies that have associated the degree of suppression of β oscillations by dopamine therapy with improvement of the hypokinetic Parkinson's disease symptoms (Kuhn *et al*., 2006, 2009; Ray *et al*., 2008). In a complementary manner, our finding that reduced low-frequency activity tended to predict the preoperative response to levodopa is in line with previous studies which have demonstrated an increase in low-frequency activity in response to levodopa and DBS (Priori *et al*., 2004, 2006). Further investigation is required as to why we did not see a relation between low-frequency activity and postoperative clinical improvement (e.g. possible differences between microelectrodes, as used in this study, versus macroelectrodes).

Although the peak frequency of β oscillations in the dorsolateral oscillatory region could be anywhere in the β range (Kuhn *et al*., 2009), previous studies have distinguished between the low-β and high-β range (Priori *et al*., 2004; Foffani *et al*., 2005; Marceglia *et al*., 2006*a*, 2009; Avila *et al*., 2010). Also in our data we see a distinction between low-β (~15 Hz) and high-β (~25 Hz). Low-β activity was dominant in the central dorsolateral oscillatory region and less evident anteriorly, whereas high-β activity was evident in both the central and anterior dorsolateral oscillatory region. Overall there was a longer dorsolateral oscillatory region and more (low and high) β oscillations in the central electrode trajectory. In our patients, mean high-β (~25 Hz) power was particularly associated with improvement in axial-bradykinesia due to DBS. In contrast, mean low-β (~15 Hz) power tended to be associated with improvement in response to medication.

The association of ~25 and ~15 Hz oscillations with DBS versus levodopa efficacy, respectively, seemed consistent in our data.

However, there are limitations when comparing several frequency bands across a single, limited dataset. Additional factors such as age, disease duration and gender differences could influence STN oscillations (Marceglia *et al*., 2006*b*). We therefore qualify that other studies on additional datasets are required to confirm these findings. In addition, multiple regression analysis across variables that are partially correlated amongst themselves, can reduce statistical power. Therefore some results may be unduly insignificant, and results or trends may really be stronger than presented.

Our association of DBS with axial symptoms versus levodopa with more distal symptoms seems to be in line with recent publications that link improvement in axial/proximal bradykinesia to DBS, and distal symptoms to levodopa (Wenzelburger *et al*., 2003; Shivitz *et al*., 2006; Timmermann *et al*., 2008). On a clinical note, whilst improvement in peripheral symptoms can be tested by stimulation during surgery, it is impractical to test axial symptoms since the patient is immobile, and the response of axial symptoms to DBS has a longer time constant (Temperli *et al*., 2003). Microelectrode recording analysis and demarcation of the dorsolateral oscillatory region during surgery may enable assessment of potential axial-bradykinesia improvement, thus affording better selection between multiple microelectrode recording tracks.

In summary, the spatial extent of the dorsolateral oscillatory region, which overlaps the motor territories of the STN, predicts the outcome of STN DBS. In addition, specific β-oscillation frequencies in the dorsolateral oscillatory region predict the response of Parkinson's disease motor symptoms to DBS and medication. We therefore suggest that optimization of DBS outcome in patients with Parkinson's disease could be achieved by intraoperative analysis of STN β oscillations by microelectrode (as in this study) or macroelectrode (Chen *et al*., 2006) recording. Optimal DBS outcome would be achieved by selecting the trajectory with maximal dorsolateral oscillatory region length and by placement of the DBS contact in proximity of the STN dorsolateral oscillatory region centre.

Acknowledgements

We would like to thank Dr E. Linetsky and E. Serri for UPDRS testing, T. Moller for help in collecting clinical data, Prof. Y. Ritov for statistical advice and A. Moran for help in data acquisition.

Funding

This work was supported by the 'Fighting against Parkinson' and the Max Vorst Family Foundations of the Hebrew University Netherlands Association (HUNA) to H.B., and the Parkinson at the Hadassah (PATH) committee of London to Z.I.

Supplementary material

Supplementary material is available at *Brain* online.

References

Amirnovin R, Williams ZM, Cosgrove GR, Eskandar EN. Visually guided movements suppress subthalamic oscillations in Parkinson's disease patients. J Neurosci 2004; 24: 11302–6.

Amtage F, Henschel K, Schelter B, Vesper J, Timmer J, Lucking CH. Hellwig B High functional connectivity of tremor related subthalamic neurons in Parkinson's disease. Clin Neurophysiol 2009; 120: 1755–61.

Avila I, Parr-Brownlie LC, Brazhnik E, Castaneda E, Bergstrom DA, Walters JR. Beta frequency synchronization in basal ganglia output during rest and walk in a hemiparkinsonian rat. Exp Neurol 2010; 221: 307–19.

Benabid AL, Chabardes S, Mitrofanis J, Pollak P. Deep brain stimulation of the subthalamic nucleus for the treatment of Parkinson's disease. Lancet Neurol 2009; 8: 67–81.

Bergman H, Wichmann T, Karmon B, DeLong MR. The primate subthalamic nucleus. II. Neuronal activity in the MPTP model of parkinsonism. J Neurophysiol 1994; 72: 507–20.

Bernheimer H, Birkmayer W, Hornykiewicz O, Jellinger K, Seitelberger F. Brain dopamine and the syndromes of Parkinson and Huntington. Clinical, morphological and neurochemical correlations. J Neurol Sci 1973; 20: 415–55.

Brown P, Oliviero A, Mazzone P, Insola A, Tonali P, Di Lazzaro V. Dopamine dependency of oscillations between subthalamic nucleus and pallidum in Parkinson's disease. J Neurosci 2001; 21: 1033–8.

Chen CC, Pogosyan A, Zrinzo LU, Tisch S, Limousin P, Ashkan K, et al. Intra-operative recordings of local field potentials can help localize the subthalamic nucleus in Parkinson's disease surgery. Exp Neurol 2006; 198: 214–21.

Costa RM, Lin SC, Sotnikova TD, Cyr M, Gainetdinov RR, Caron MG, et al. Rapid alterations in corticostriatal ensemble coordination during acute dopamine-dependent motor dysfunction. Neuron 2006; 52: 359–69.

Fahn S, Elton RL. Unified Parkinson's Disease Rating Scale. In: Fahn S, Marsden CD, Goldstein M, Calne DB, editors. UPDRS program members. Recent developments in Parkinson's disease. Florham Park, NJ: Macmillan Healthcare Information; 1987. p. 153–163, 293–304.

Filion M, Tremblay L. Abnormal spontaneous activity of globus pallidus neurons in monkeys with MPTP-induced parkinsonism. Brain Res 1991; 547: 142–51.

Foffani G, Ardolino G, Egidi M, Caputo E, Bossi B, Priori A. Subthalamic oscillatory activities at beta or higher frequency do not change after high-frequency DBS in Parkinson's disease. Brain Res Bull 2006; 69: 123–30.

Foffani G, Bianchi AM, Baselli G, Priori A. Movement-related frequency modulation of beta oscillatory activity in the human subthalamic nucleus. J Physiol 2005; 568: 699–711.

Godinho F, Thobois S, Magnin M, Guenot M, Polo G, Benatru I, et al. Subthalamic nucleus stimulation in Parkinson's disease: anatomical and electrophysiological localization of active contacts. J Neurol 2006; 253: 1347–55.

Gross RE, Krack P, Rodriguez-Oroz MC, Rezai AR, Benabid AL. Electrophysiological mapping for the implantation of deep brain stimulators for Parkinson's disease and tremor. Mov Disord 2006; 21(Suppl 14): S259–83.

Herzog J, Fietzek U, Hamel W, Morsnowski A, Steigerwald F, Schrader B, et al. Most effective stimulation site in subthalamic deep brain stimulation for Parkinson's disease. Mov Disord 2004; 19: 1050–4.

Herzog J, Pinsker M, Wasner M, Steigerwald F, Wailke S, Deuschl G, et al. Stimulation of subthalamic fibre tracts reduces dyskinesias in STN-DBS. Mov Disord 2007; 22: 679–84.

Hutchison WD, Allan RJ, Opitz H, Levy R, Dostrovsky JO, Lang AE, et al. Neurophysiological identification of the subthalamic nucleus in surgery for Parkinson's disease. Ann Neurol 1998; 44: 622–8.

Israel Z, Burchiel K. Microelectrode recording in movement disorder surgery. Stuttgart: Thieme; 2004.

Krack P, Batir A, Van Blercom N, Chabardes S, Fraix V, Ardouin C, et al. Five-year follow-up of bilateral stimulation of the subthalamic nucleus in advanced Parkinson's disease. N Engl J Med 2003; 349: 1925–34.

Kuhn AA, Kempf F, Brucke C, Gaynor DL, Martinez-Torres I, Pogosyan A, et al. High-frequency stimulation of the subthalamic nucleus suppresses oscillatory beta activity in patients with Parkinson's disease in parallel with improvement in motor performance. J Neurosci 2008; 28: 6165–73.

Kuhn AA, Kupsch A, Schneider GH, Brown P. Reduction in subthalamic 8-35 Hz oscillatory activity correlates with clinical improvement in Parkinson's disease. Eur J Neurosci 2006; 23: 1956–60.

Kuhn AA, Trottenberg T, Kivi A, Kupsch A, Schneider GH, Brown P. The relationship between local field potential and neuronal discharge in the subthalamic nucleus of patients with Parkinson's disease. Exp Neurol 2005; 194: 212–20.

Kuhn AA, Tsui A, Aziz T, Ray N, Brucke C, Kupsch A, et al. Pathological synchronisation in the subthalamic nucleus of patients with Parkinson's disease relates to both bradykinesia and rigidity. Exp Neurol 2009; 215: 380–7.

Levy R, Ashby P, Hutchison WD, Lang AE, Lozano AM, Dostrovsky JO. Dependence of subthalamic nucleus oscillations on movement and dopamine in Parkinson's disease. Brain 2002; 125: 1196–209.

Levy R, Hutchison WD, Lozano AM, Dostrovsky JO. High-frequency synchronization of neuronal activity in the subthalamic nucleus of parkinsonian patients with limb tremor. J Neurosci 2000; 20: 7766–75.

Limousin P, Pollak P, Benazzouz A, Hoffmann D, Broussolle E, Perret JE, et al. Bilateral subthalamic nucleus stimulation for severe Parkinson's disease. Mov Disord 1995; 10: 672–4.

Lujan JL, Noecker AM, Butson CR, Cooper SE, Walter BL, Vitek JL, et al. Automated 3-dimensional brain atlas fitting to microelectrode recordings from deep brain stimulation surgeries. Stereotact Funct Neurosurg 2009; 87: 229–40.

Machado A, Rezai AR, Kopell BH, Gross RE, Sharan AD, Benabid AL. Deep brain stimulation for Parkinson's disease: Surgical technique and perioperative management. Mov Disord 2006; 21: S247–58.

Magill PJ, Bolam JP, Bevan MD. Dopamine regulates the impact of the cerebral cortex on the subthalamic nucleus-globus pallidus network. Neuroscience 2001; 106: 313–30.

Magill PJ, Sharott A, Bolam JP, Brown P. Delayed synchronization of activity in cortex and subthalamic nucleus following cortical stimulation in the rat. J Physiol 2006; 574: 929–46.

Maks CB, Butson CR, Walter BL, Vitek JL, McIntyre CC. Deep brain stimulation activation volumes and their association with neurophysiological mapping and therapeutic outcomes. J Neurol Neurosurg Psychiatry 2009; 80: 659–66.

Marceglia S, Fiorio M, Foffani G, Mrakic-Sposta S, Tiriticco M, Locatelli M, et al. Modulation of beta oscillations in the subthalamic area during action observation in Parkinson's disease. Neuroscience 2009; 161: 1027–36.

Marceglia S, Foffani G, Bianchi A, Baselli G, Tamma F, Egidi M, et al. Dopamine-dependent non-linear correlation between subthalamic rhythms in Parkinson's disease. J Physiol 2006a; 571: 579–91.

Marceglia S, Mrakic-Sposta S, Foffani G, Cogiamanian F, Caputo E, Egidi M, et al. Gender-related differences in the human subthalamic area: a local field potential study. Eur J Neurosci 2006b; 24: 3213–22.

Miller WC, DeLong MR. Altered tonic activity of neurons in the globus pallidus and subthalamic nucleus in the primate MPTP model of parkinsonism. In: Carpenter MB, Jayaraman A, editors. The basal ganglia II. New York: Plenum Press; 1987. p. 415–427.

Mogilner AY, Sterio D, Rezai AR, Zonenshayn M, Kelly PJ, Beric A. Subthalamic nucleus stimulation in patients with a prior pallidotomy. J Neurosurg 2002; 96: 660–5.

Monakow KH, Akert K, Kunzle H. Projections of the precentral motor cortex and other cortical areas of the frontal lobe to the subthalamic nucleus in the monkey. Exp Brain Res 1978; 33: 395–403.

Moran A, Bar-Gad I. Revealing neuronal functional organization through the relation between multi-scale oscillatory extracellular signals. J Neurosci Methods 2010; 186: 116–29.

Moran A, Bar-Gad I, Bergman H, Israel Z. Real-time refinement of subthalamic nucleus targeting using Bayesian decision-making on the root mean square measure. Mov Disord 2006; 21: 1425–31.

Moran A, Bergman H, Israel Z, Bar-Gad I. Subthalamic nucleus functional organization revealed by parkinsonian neuronal oscillations and synchrony. Brain 2008; 131: 3395–409.

Nambu A, Takada M, Inase M, Tokuno H. Dual somatotopical representations in the primate subthalamic nucleus: evidence for ordered but reversed body-map transformations from the primary motor cortex and the supplementary motor area. J Neurosci 1996; 16: 2671–83.

Nini A, Feingold A, Slovin H, Bergman H. Neurons in the globus pallidus do not show correlated activity in the normal monkey, but phase-locked oscillations appear in the MPTP model of parkinsonism. J Neurophysiol 1995; 74: 1800–5.

Priori A, Ardolino G, Marceglia S, Mrakic-Sposta S, Locatelli M, Tamma F, et al. Low-frequency subthalamic oscillations increase after deep brain stimulation in Parkinson's disease. Brain Res Bull 2006; 71: 149–54.

Priori A, Foffani G, Pesenti A, Bianchi A, Chiesa V, Baselli G, et al. Movement-related modulation of neural activity in human basal ganglia and its L-DOPA dependency: recordings from deep brain stimulation electrodes in patients with Parkinson's disease. Neurol Sci 2002; 23(Suppl 2): S101–2.

Priori A, Foffani G, Pesenti A, Tamma F, Bianchi AM, Pellegrini M, et al. Rhythm-specific pharmacological modulation of subthalamic activity in Parkinson's disease. Exp Neurol 2004; 189: 369–79.

Ray NJ, Jenkinson N, Wang S, Holland P, Brittain JS, Joint C, et al. Local field potential beta activity in the subthalamic nucleus of patients with Parkinson's disease is associated with improvements in bradykinesia after dopamine and deep brain stimulation. Exp Neurol 2008; 213: 108–13.

Reck C, Florin E, Wojtecki L, Krause H, Groiss S, Voges J, et al. Characterisation of tremor-associated local field potentials in the subthalamic nucleus in Parkinson's disease. Eur J Neurosci 2009; 29: 599–612.

Rodriguez-Oroz MC, Rodriguez M, Guridi J, Mewes K, Chockkman V, Vitek J, et al. The subthalamic nucleus in Parkinson's disease: somatotopic organization and physiological characteristics. Brain 2001; 124: 1777–90.

Romanelli P, Esposito V, Schaal DW, Heit G. Somatotopy in the basal ganglia: experimental and clinical evidence for segregated sensorimotor channels. Brain Res Brain Res Rev 2005; 48: 112–28.

Rossi L, Marceglia S, Foffani G, Cogiamanian F, Tamma F, Rampini P, et al. Subthalamic local field potential oscillations during ongoing deep brain stimulation in Parkinson's disease. Brain Res Bull 2008; 76: 512–21.

Shivitz N, Koop MM, Fahimi J, Heit G, Bronte-Stewart HM. Bilateral subthalamic nucleus deep brain stimulation improves certain aspects of postural control in Parkinson's disease, whereas medication does not. Mov Disord 2006; 21: 1088–97.

Steigerwald F, Potter M, Herzog J, Pinsker M, Kopper F, Mehdorn H, et al. Neuronal activity of the human subthalamic nucleus in the parkinsonian and nonparkinsonian state. J Neurophysiol 2008; 100: 2515–24.

Sterio D, Zonenshayn M, Mogilner AY, Rezai AR, Kiprovski K, Kelly PJ, et al. Neurophysiological refinement of subthalamic nucleus targeting. Neurosurgery 2002; 50: 58–67.

Temperli P, Ghika J, Villemure JG, Burkhard PR, Bogousslavsky J, Vingerhoets FJ. How do parkinsonian signs return after discontinuation of subthalamic DBS? Neurology 2003; 60: 78–81.

Theodosopoulos PV, Marks WJ Jr, Christine C, Starr PA. Locations of movement-related cells in the human subthalamic nucleus in Parkinson's disease. Mov Disord 2003; 18: 791–8.

Timmermann L, Braun M, Groiss S, Wojtecki L, Ostrowski S, Krause H, et al. Differential effects of levodopa and subthalamic nucleus deep brain stimulation on bradykinesia in Parkinson's disease. Mov Disord 2008; 23: 218–27.

Trottenberg T, Kupsch A, Schneider GH, Brown P, Kuhn AA. Frequency-dependent distribution of local field potential activity within the subthalamic nucleus in Parkinson's disease. Exp Neurol 2007; 205: 287–91.

Weinberger M, Hutchison WD, Dostrovsky JO. Pathological subthalamic nucleus oscillations in PD: Can they be the cause of bradykinesia and akinesia? Exp Neurol 2009; 219: 58–61.

Weinberger M, Mahant N, Hutchison WD, Lozano AM, Moro E, Hodaie M, et al. Beta oscillatory activity in the subthalamic nucleus and its relation to dopaminergic response in Parkinson's disease. J Neurophysiol 2006; 96: 3248–56.

Wenzelburger R, Kopper F, Zhang BR, Witt K, Hamel W, Weinert D, et al. Subthalamic nucleus stimulation for Parkinson's disease preferentially improves akinesia of proximal arm movements compared to finger movements. Mov Disord 2003; 18: 1162–9.

Wichmann T, Bergman H, DeLong MR. The primate subthalamic nucleus. I. Functional properties in intact animals. J Neurophysiol 1994; 72: 494–506.

Wingeier B, Tcheng T, Koop MM, Hill BC, Heit G, Bronte-Stewart HM. Intra-operative STN DBS attenuates the prominent beta rhythm in the STN in Parkinson's disease. Exp Neurol 2006; 197: 244–51.

Zaidel A, Moran A, Marjan G, Bergman H, Israel Z. Prior pallidotomy reduces and modifies neuronal activity in the subthalamic nucleus of Parkinson's disease patients. Eur J Neurosci 2008; 27: 483–91.

Zaidel A, Spivak A, Shpigelman L, Bergman H, Israel Z. Delimiting subterritories of the human subthalamic nucleus by means of microelectrode recordings and a Hidden Markov Model. Mov Disord 2009; 24: 1785–93.